

Nonlinear analysis of the Eckhaus instability: modulated amplitude waves and phase chaos with nonzero average phase gradient

Lutz Brusch^a, Alessandro Torcini^{b,c}, Markus Bär^{a,*}

^a *Max-Planck-Institut für Physik komplexer Systeme, Nöthnitzer Straße 38, D-01187 Dresden, Germany*

^b *Dipartimento di Energetica, Università di Firenze, via S. Marta 3, I-50139 Firenze, Italy*

^c *Istituto Nazionale di Ottica Applicata, L.go E. Fermi 6, I-50125 Firenze, Italy*

Received 22 October 2001; received in revised form 24 March 2002; accepted 5 April 2002

Abstract

We analyze the Eckhaus instability of plane waves in the one-dimensional complex Ginzburg–Landau equation (CGLE) and describe the nonlinear effects arising in the Eckhaus unstable regime. Modulated amplitude waves (MAWs) are quasi-periodic solutions of the CGLE that emerge near the Eckhaus instability of plane waves and cease to exist due to saddle-node (SN) bifurcations. These MAWs can be characterized by their average phase gradient ν and by the spatial period P of the periodic amplitude modulation. A numerical bifurcation analysis reveals the existence and stability properties of MAWs with arbitrary ν and P . MAWs are found to be stable for large enough ν and intermediate values of P . For different parameter values they are unstable to splitting and attractive interaction between subsequent extrema of the amplitude. Defects form from perturbed plane waves for parameter values above the SN of the corresponding MAWs. The break-down of phase chaos with average phase gradient $\nu \neq 0$ (“wound-up phase chaos”) is thus related to these SNs. A lower bound for the break-down of wound-up phase chaos is given by the necessary presence of SNs and an upper bound by the absence of the splitting instability of MAWs.

© 2002 Elsevier Science B.V. All rights reserved.

PACS: 05.45.Jn; 03.40.Kf; 05.45.–a

Keywords: Complex Ginzburg–Landau equation; Coherent structures; Modulated amplitude waves; Phase chaos

1. Introduction

The emergence of chaotic behaviour from ordered states in spatially extended systems has been the subject of many recent experimental and theoretical investigations [1,2]. Nonetheless, the mechanisms leading from stationary regimes to chaotic (or spatially irregu-

lar) phases still pose many challenging questions. One of the most studied instabilities in extended oscillatory systems is the Eckhaus instability of plane waves [3].

The occurrence of this instability has been experimentally observed in many quasi one-dimensional systems like the oscillatory instability of a Rayleigh–Bénard convection pattern [4], hydrothermal waves [5–8], heated wire convection [9], sidewall convection [10], the Taylor–Dean system [11] and internal waves

* Corresponding author. Tel.: +49-351-871-2218;
fax: +49-351-871-1999.
E-mail address: baer@mpipks-dresden.mpg.de (M. Bär).

excited by the Marangoni effect [12]. The Eckhaus instability also plays an important role in the radial dynamics of spiral waves in the Belousov–Zhabotinsky reaction [13].

The complex Ginzburg–Landau equation (CGLE) [2,14] is the appropriate amplitude equation to describe the slow dynamics near a supercritical transition to unidirectional traveling waves. In one spatial dimension, the CGLE reads

$$\partial_t A = A + (1 + ic_1)\partial_x^2 A - (1 - ic_3)|A|^2 A, \quad (1)$$

where c_1 and c_3 are real coefficients and the field $A = A(x, t) = |A(x, t)|e^{i\varphi(x, t)}$ has complex values. As exact solutions the CGLE admits plane waves of the form $A_q(x, t) = a_q e^{i(qx - \omega_q t)}$, where q indicates the wavenumber, $a_q = \sqrt{1 - q^2}$ and $\omega_q = -c_3 + q^2(c_1 + c_3)$.

A linear stability analysis [15] of these solutions can be performed by considering the perturbed solution $\tilde{A}_q(x, t) = (a_q + \delta a)e^{i(qx - \omega_q t)}$, where $\delta a \propto e^{ikx} e^{\sigma(k)t}$. The growth rates associated to the complex perturbation δa is

$$\sigma(k) = -k^2 - 2iqc_1k - (1 - q^2) \pm \{(1 + c_3^2)(1 - q^2)^2 - [c_1k^2 - 2iqk - c_3(1 - q^2)]^2\}^{1/2}. \quad (2)$$

The plane waves become linearly unstable to long wavelength perturbations ($k \rightarrow 0$) for $q = q_E \equiv \sqrt{(1 - c_1c_3)/(2(1 + c_3^2) + 1 - c_1c_3)}$. This limit is called Eckhaus instability [3]. Above the Benjamin–Feir–Newell (BFN) line $1 - c_1c_3 = 0$, all plane waves are unstable to homogeneous perturbations. For a given $q \geq q_E$, the corresponding plane wave is linearly unstable against perturbations with wavenumbers k inside the interval $0 < |k| < k_c$. k_c increases for increasing values of the parameters c_1 and c_3 .¹

As noticed in [16,17], the Eckhaus instability is a convective instability. Thus, it is relevant in the systems with periodic boundary conditions considered

here, while it would be suppressed in fixed boundary conditions, e.g. zero-flux or Dirichlet boundary conditions. In the latter geometries, the absolute instability of the plane waves has to be computed. It occurs for sufficiently large q and/or c_1, c_3 values inside the Eckhaus unstable range.

Another interesting aspect of the Eckhaus instability is found when the nonlinearities of the CGLE are taken into account. A weakly nonlinear analysis [4] revealed that for

$$c_1^2(1 - 6c_3^2) + c_1(2c_3^3 + 16c_3) - (8 + c_3^2) > 0, \quad (3)$$

the Eckhaus instability becomes supercritical, i.e. the instabilities are saturated and the emerging quasi-periodic solutions coexist with the unstable plane waves of uniform amplitude [18]. We call these quasi-periodic solutions modulated amplitude waves (MAWs). Series expansions of the MAWs [19,20] and their linear stability properties within a phase approximation near the Eckhaus instability [21,22] have been obtained. Numerical simulations [4,23–26] provided examples of stable MAWs. They have also been observed in experiments on surface-tension-driven hydrothermal waves [6] as well as on the Taylor–Dean system [11] and on internal waves excited by the Marangoni effect [12].

In addition, the CGLE exhibits two qualitatively different spatiotemporal chaotic states known as phase chaos (when the modulus of the field $|A|$ is bounded away from zero) and defect chaos (when the phase of A displays singularities where $|A| = 0$) [27–30]. The subclass of MAWs with zero average phase gradient is important for understanding the transition from phase to defect chaos (see solid curve in Fig. 1) [31,32]. In the phase chaos regime states with nonzero average phase gradient ν have a dynamics quite different from that at $\nu \sim 0$. In particular, these states can be either chaotic or regular depending on the initial conditions and on the parameters c_1, c_3 and ν . In this paper we will focus on MAWs with $\nu \neq 0$ and on the dynamical regime associated to them, that is referred to as “wound-up” phase chaos [24]. It will be shown that MAWs and wound-up phase chaos exist between the dashed and the solid curves in Fig. 1.

¹ The perturbation with wavenumber k_c of a plane wave q travels with a velocity $v_c = -\text{Im}[\sigma(k_c)]/k_c$. At the Eckhaus instability, in the infinite system, $k_c \rightarrow 0$ and v_c equals the group velocity $v_g = \partial\omega_q/\partial q = 2q(c_1 + c_3)$. For finite system size $k_c > 0$ and $v_c \neq v_g$.

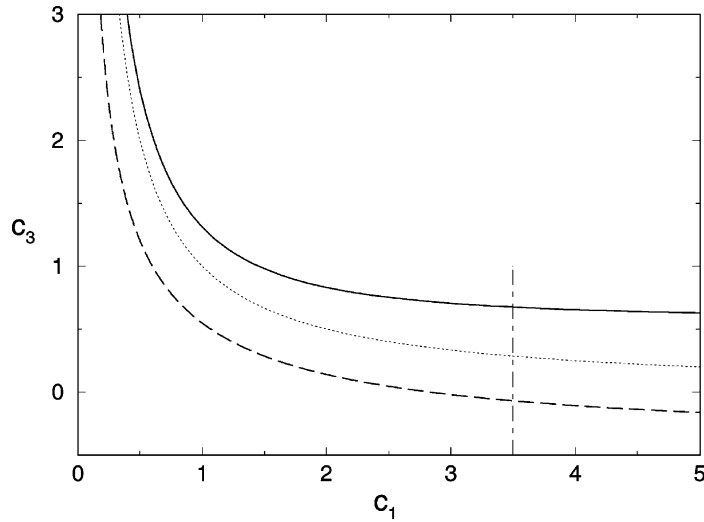


Fig. 1. Phase diagram of the CGLE. The dotted curve indicates the BFN line. Plane waves undergo an Eckhaus instability at values of c_1, c_3 below this curve depending on their wavenumber. Above the dashed curve the Eckhaus instability is supercritical, whereas it is subcritical below [4]. MAWs and wound-up phase chaos with $\nu > 0$ can be observed between the dashed and the solid curves. Defect chaos can occur only above the solid curve [31,32] which denotes the saddle-node (SN) bifurcation of MAWs with $\nu = 0$ and $P \rightarrow \infty$. The vertical dot-dashed line indicates the cut of the parameter space at $c_1 = 3.5$ studied in this paper.

In Section 2 the analysis of MAWs introduced in [31,32] is extended to arbitrary values of the average phase gradients of the field. The two parameter family of MAW solutions is parametrized by the spatial period P of the modulation and by the average phase gradient

$$\nu := \frac{1}{P} \int_0^P dx \varphi_x. \quad (4)$$

For plane wave solutions, ν equals the wavenumber q . In analogy, the phase gradient φ_x is often called “local wavenumber”. A linear stability analysis will show that MAWs with $\nu \neq 0$ can be stable even in infinitely large systems. For systems with periodic boundary conditions the average phase gradient of the whole system can only be changed, if a space–time defect occurs: $|A(x, t)|$ drops to zero and φ_x locally diverges at a defect. Persistent phase chaos with conserved $\nu \leq \nu_M \neq 0$ has been observed in numerical simulations of the CGLE (1) [24,25]. The maximum conserved average phase gradient ν_M decreases as function of the coefficients c_1, c_3 [24,25] and vanishes at the apparent transition from phase to defect

chaos. ν_M was therefore suggested [25] as an order parameter for this transition. We extended the numerical determination of ν_M towards smaller c_3 and report the corresponding data in Fig. 2.

In Section 3, a nonlinear analysis of the Eckhaus instability allows to estimate the parameter values for which defects occur. Lower and upper bounds for the limit ν_M of wound-up phase chaos are derived from the existence and stability properties of the MAWs. For increasing ν the degree of chaoticity associated with the wound-up phase chaos decreases [25]. For large enough ν the dynamics can even become regular and stable quasi-periodic MAWs appear. The diamonds in Fig. 2 indicate this stability limit for numerical simulations with fixed $c_1 = 3.5$. The analysis in Section 2.3 will clarify this observation.

The large number of parameters (c_1, c_3, ν, P) calls for restrictions. We limit our analysis to fixed $c_1 = 3.5$ since most previous numerical work has been done at this value [25,30]. The results will be presented as projections of the P direction onto the (c_3, ν) plane as well as in cuts through the parameter space spanned by c_3, ν , and P . Additional investigations of the

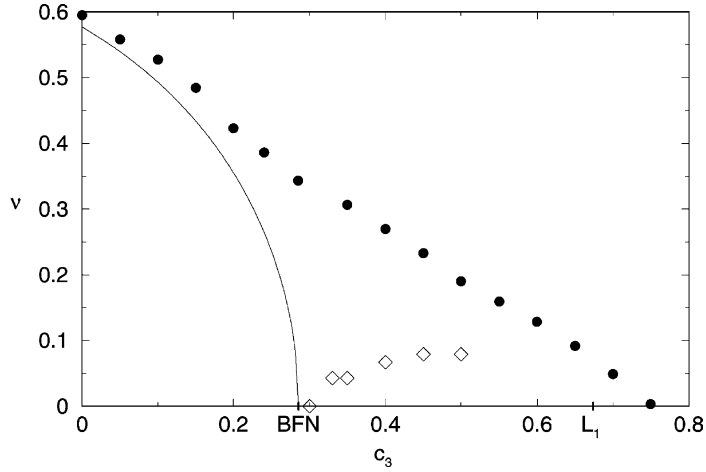


Fig. 2. Maximum (filled circles) conserved average phase gradient $v_M(c_3)$ for fixed $c_1 = 3.5$ obtained from numerical simulations (with system size $L = 1024$ – 2048 and integration times $t \sim 10^5$) for 50–70 different initial conditions (noise added to plane wave with wavenumber $q = v$). For $v \leq v_M$ no defects were present while above v_M at least one initial condition caused defects. The solid curve denotes the Eckhaus instability of plane waves that converges to the BFN line at $c_3 = 1/c_1$ for $v = 0$. For v above the diamonds regular states were observed after a transient phase chaotic dynamics but below the diamonds most initial conditions led to persistent spatio-temporal chaos [25]. L_1 denotes the lower bound for the occurrence of defect chaos in the thermodynamic limit as calculated in [31,32].

existence domains of MAWs revealed qualitatively similar results for fixed $c_1 = 0.4, 1.2, 2.1,$ and 5 and variable c_3 as well as for fixed $c_3 = 0.83$ and variable c_1 . Two of these choices were studied by numerical simulations in [24]. A similarity transformation maps coherent structures onto each other along curves $(c_1 + c_3)/(1 - c_1 c_3) = \text{const.}$ in coefficient space [14]. The parameters ν, P, ω, v are transformed accordingly. One can thereby extend the results presented here to other values of the coefficient c_1 . Section 4 discusses possible observations of MAWs in experimental systems. Finally, Section 5 summarizes the main results.

2. Existence and stability of MAWs

2.1. Coherent structure approach

In analogy to the linear stability analysis of plane waves we make the following ansatz for saturated modulations:

$$A(x, t) = a(z) e^{i\tilde{\phi}(z)} e^{i(qx - \tilde{\omega}t)}, \quad (5)$$

and rewrite it as

$$A(x, t) = a(z) e^{i\phi(z)} e^{i\omega t}, \quad (6)$$

where a and ϕ are real-valued functions of $z := x - vt$ and $\phi(z) = \tilde{\phi}(z) + qz$, and $\omega = qv - \tilde{\omega}$. Here $a(z)$ and $\phi(z)$ represent coherent structures [33]. Coherent structures have been studied extensively [25,31–34] and play an important role in various regimes of the CGLE [4,23–25,31–35].

Substitution of ansatz (6) into the CGLE (1) yields the set of three coupled nonlinear ordinary differential equations (ODEs):

$$\begin{aligned} a_z &= b, \\ b_z &= \psi^2 a - \gamma^{-1} [(1 + c_1 \omega) a + v(b + c_1 \psi a) \\ &\quad - (1 - c_1 c_3) a^3], \\ \psi_z &= -\frac{2b\psi}{a} \\ &\quad + \gamma^{-1} \left[c_1 - \omega + v \left(\frac{c_1 b}{a} - \psi \right) - (c_1 + c_3) a^2 \right], \end{aligned} \quad (7)$$

where $b := a_z, \psi := \phi_z$ and $\gamma := 1 + c_1^2$.² The continuation software AUTO97 [36] is used to compute the periodic orbits of the ODEs (7) that correspond to spatially periodic functions $a(z)$ and $\phi(z)$.

² By substituting $\kappa := a_z/a$ one reproduces the form of the ODEs used in [33] which is more appropriate for studies of fronts.

In order to choose a unique solution from the continuous two-parameter family of periodic orbits we set the system size L equal to the period P of the periodic orbit and fix its average phase gradient by $\nu = 1/L \int_0^L \psi \, dz$.

The continuation procedure starts from a fixed point $(a, b, \psi) = (\sqrt{1 - q^2}, 0, q)$ that corresponds to a plane wave solution. Varying c_3 , a Hopf bifurcation (HB) (filled square in Fig. 3) is detected in the ODEs where the mode with the smallest possible wave number $k_{\text{HB}} = 2\pi/P$ destabilizes the plane wave. Continuing the resulting branch of MAWs the free parameters ω and ν are adjusted by the continuation algorithm. The continuation follows a unique branch of MAWs with $\nu = q$ and $P = L$. Fig. 3 shows examples of resulting bifurcation diagrams.

2.2. Existence limits of MAWs

Upon increasing of c_3 amplitude modulations grow and develop a localized depression $|A|_{\text{min}}$ where ϕ_x has a maximum (see Fig. 3b and c). As for $\nu = 0$, these MAWs are called the *lower branch* in contrast to the coexisting *upper branch* MAWs. The upper branch MAWs are always unstable, while the MAWs of the lower branch can be stable in appropriate parameter regions. Examples of these lower branch MAWs have been obtained by numerical simulations earlier [4,23–25]. They have been analyzed in detail in [26]. Numerical simulations can neither uncover unstable upper branch MAWs nor elucidate the limits of existence of MAWs. The bifurcation analysis presented here reveals that upper and lower branch meet and

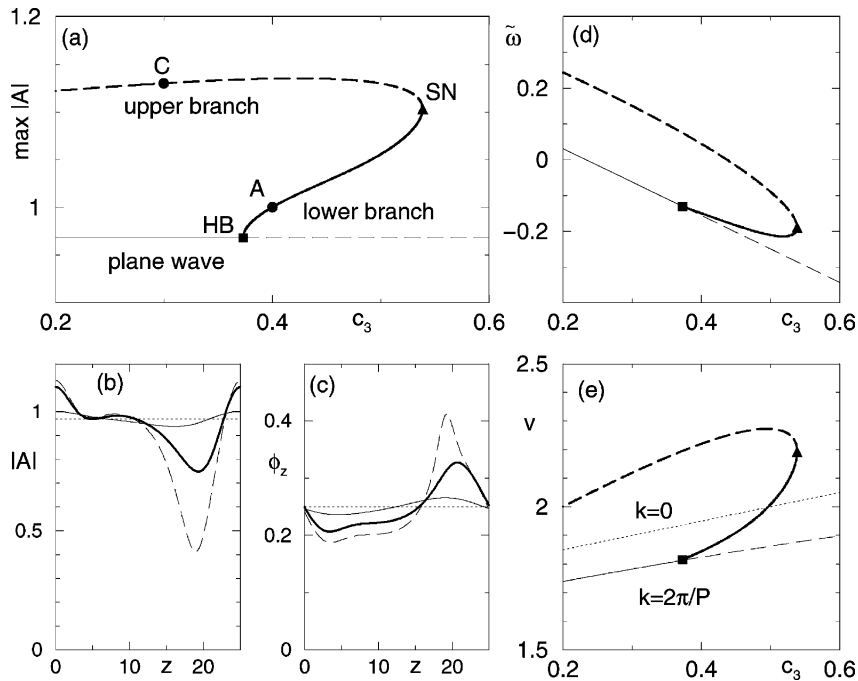


Fig. 3. (a) Example of a bifurcation diagram showing the maximum of the modulus for MAWs with $\nu = 0.25, c_1 = 3.5$, and $P = 2\pi/\nu = 25.13$. The plane wave that is stable (unstable) against modes of wavelength P is represented by the thin solid (dashed) line. The stable lower branch (unstable upper branch) of MAWs is denoted by the thick solid (dashed) curve. HB denotes the Hopf bifurcation (square) of the plane wave solution, whereas SN stands for the saddle-node bifurcation (triangle) that limits the existence of MAWs. Spatial portraits of (b) the modulus and (c) the phase gradient are shown for a choice of solutions. The dotted line represents the plane wave, whereas thin solid and thick solid curves give MAWs at locations labeled by A and SN in (a). The dashed curve denotes the saddle-type upper branch solution at C in (a). (d) shows the oscillation frequency $\tilde{\omega} = q\nu - \omega$ and (e) the velocity ν vs. c_3 . In (e) the dotted line denotes the group velocity ($k = 0$) and the line below gives the velocity ν_c corresponding to the mode with finite wavelength P (see Footnote 1).

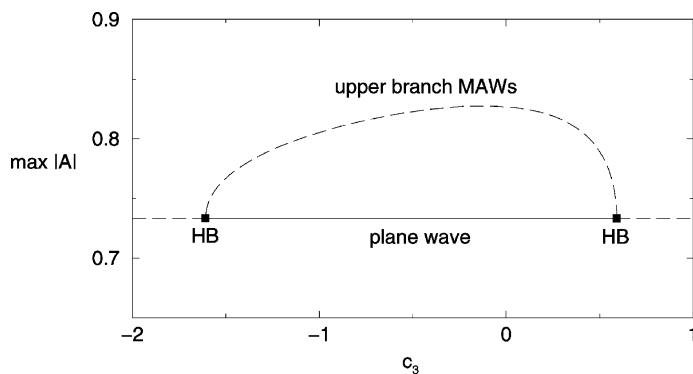


Fig. 4. Bifurcation diagram with exclusive upper branch MAWs for $\nu = 0.68$ and $P = 2\pi/\nu \approx 9.24$. The solid line indicates stable and the dashed curve unstable solutions. HBs are both subcritical.

terminate in a SN bifurcation (filled triangle in Fig. 3a, d and e). Due to the SN bifurcation the upper branch MAWs always have at least one unstable eigenmode, see also [34,35]. The upper branch continues to negative c_3 and there connects to another instability of the plane wave with identical ν and P . In the following we will concentrate on the lower branch MAWs.

For large ν and small P , HB is no longer supercritical and an unstable branch emerges directly from the plane wave. This is in agreement with analytical predictions [4]. Fig. 4 shows an example which also includes the second HB at negative c_3 . For $\nu = 0$ the MAWs emerge stationary [31,32] and acquire $\nu \neq 0$

above a subsequent drift pitchfork (DP) bifurcation [37]. In the present case $\nu \neq 0$ the plane wave already breaks the reflection symmetry, the initial MAW has a nonzero velocity and the DP bifurcation (filled diamond) is unfolded. See Fig. 5 for an example at fixed $c_3 = 2$. The branch emerging at the HB in Fig. 5b represents the MAWs as discussed above. The second branch in Fig. 5b emerges at the period doubling (PD) bifurcation (open square) of MAWs with half the period. It always has unstable eigenmodes that drive the dynamics away from it to the coexisting MAWs of shorter period. Therefore this (upper) branch plays no essential role and is not treated further.

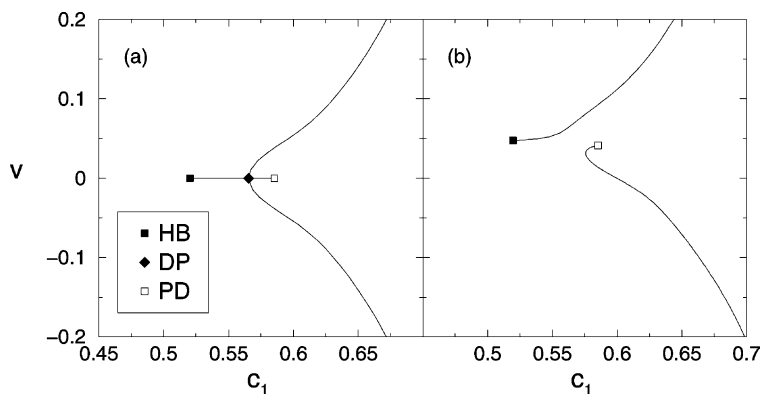


Fig. 5. Bifurcation diagrams showing the velocity v vs. c_1 . (a) Branches with $v \neq 0$ emerge at the DP bifurcation for $c_3 = 2$, $P = 25$, and $\nu = 0$. (b) The bifurcation is unfolded for $\nu \neq 0$, here $c_3 = 2$, $P = 25$, and $\nu = 0.01$. An equivalent pair of branches exists for $\nu \rightarrow -\nu$ and $v \rightarrow -v$.

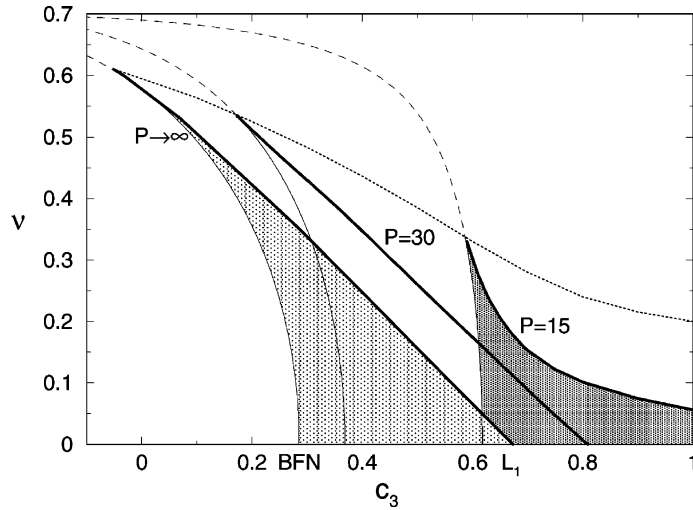


Fig. 6. Existence domains of MAWs with period P projected onto the (c_3, ν) parameter plane. Thin curves denote the HB for various P which occurs supercritical (solid curve) or subcritical (dashed curve) depending on ν and P . The left most of these curves corresponds to the Eckhaus instability ($P \rightarrow \infty$). The thick curves give the SN for selected periods P . Three examples of existence domains for $P = 15$ (right, dark shaded domain), $P = 30$ (middle, empty domain), and $P \rightarrow \infty$ (left, light shaded domain) are shown. The superposition of all existence domains is bounded by the dotted curve.

2.2.1. Infinite system size

We have analyzed the existence of lower branch MAWs in the entire parameter space (c_3, ν, P) at fixed $c_1 = 3.5$. The system size is assumed infinitely large in order to allow for arbitrary periods P of MAWs. Fig. 6 shows examples of existence domains for $P = 15$, $P = 30$, and $P \rightarrow \infty$. We find that both HB and SN shift to larger c_3 as the period P is decreased. The same behavior has already been observed in the special case $\nu = 0$ [31,32]. The dotted curve in Fig. 6 indicates the “envelope” of all SN bifurcations for MAWs of any period and therefore is the upper boundary for the existence domain of the MAWs.

2.2.2. Medium system size

Experimental setups and numerical simulations are restricted to finite system size L . Often periodic boundary conditions (corresponding to an annular geometry) are used in order to study bulk effects of extended systems and to minimize boundary effects. The periodic boundary conditions also restrict possible modes of perturbations. As described by Eq. (2) the instability threshold of plane wave solutions depends

on the wavenumber k of the perturbation. Since in the studied range of coefficients the Eckhaus instability is a long-wavelength instability the plane waves will be stabilized in small systems. The instability threshold is shifted to larger values of the coefficients c_1, c_3 and can be computed from Eq. (2) setting $k = 2\pi/L$.

Clearly the selection of perturbations by periodic boundary conditions also restricts possible MAWs. Their average phase gradient ν and the period P have to be consistent with the system size and this renders the two-parameter family of MAWs discrete. It is thus convenient to parametrize MAWs by the average phase gradient ν and the ratio n of wavelength

$$n := \frac{P}{2\pi/\nu}. \quad (8)$$

The ratio n takes values of integer fractions where the nominator counts the number of underlying wave length and the denominator the number of humps of the modulation. Hence this quantity is easily accessible in experiments. The existence domains of MAWs with respective n are presented in the (c_3, ν) parameter plane in Fig. 7.

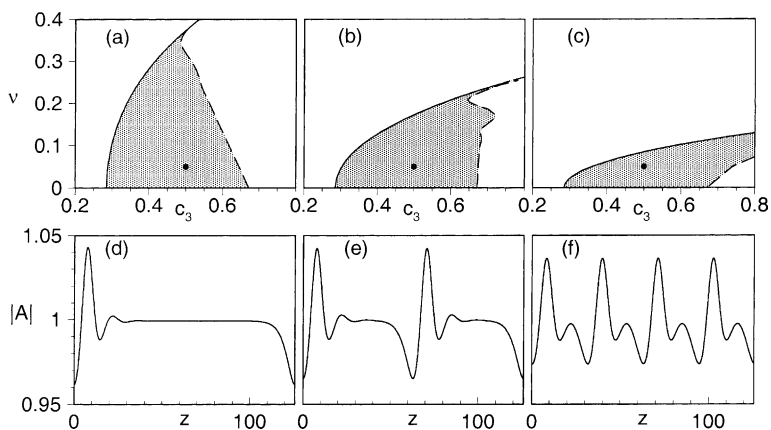


Fig. 7. Existence domains of lower branch MAWs are denoted by shaded areas for (a) $n = 1$, (b) $n = 1/2$, and (c) $n = 1/4$. They are limited by HB (solid curve) at small c_3 and by the SN (dashed curve) at large c_3 . Spatial profiles of coexisting MAWs at $\nu = 0.05$, $c_3 = 0.5$ are shown for (d) $n = 1$, (e) $n = 1/2$, and (f) $n = 1/4$, corresponding to filled circles in (a)–(c).

2.2.3. Small system size

Here we focus on the extreme case. The shortest possible system with periodic boundary conditions only contains one wavelength of the plane wave, consequently its length L is given by $L = 2\pi/\nu$. In [25] the quantity ν_U was determined in analogy to ν_M for large systems. ν_U denotes the largest ν for which none

of the random initial conditions (different realizations of noise added to a plane wave) produced a defect. In the following these data (symbols in Fig. 8) are compared to the existence domains of MAWs.

Within the light shaded area in Fig. 8 plane wave solutions with wavenumber ν are stable in the short system. The stability area extends over the phase chaos

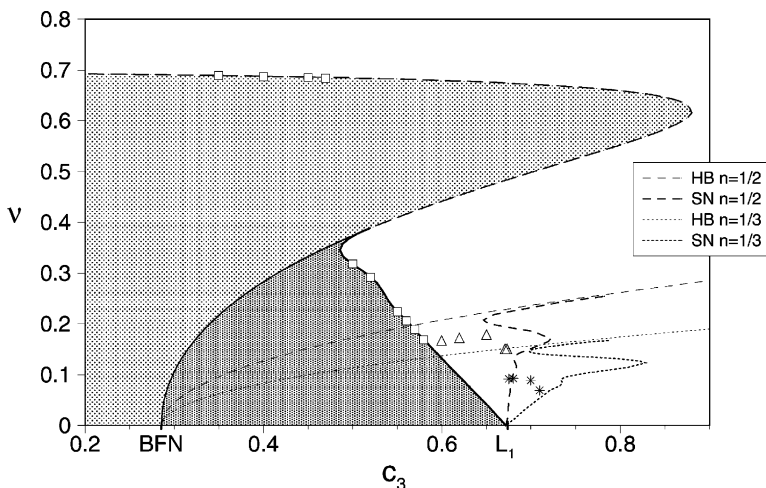


Fig. 8. For short system size $L = 2\pi/\nu$ plane waves are stable for parameter choices inside the light shaded area. MAWs with a single hump ($P = L$) exist inside the dark shaded area bounded by the supercritical HB to the left and the SN to the right. Thin curves give the limits of MAWs with two humps $P = L/2$ (dashed curve) and three humps $P = L/3$ (dotted curve). See the legend for the different cases. Symbols denote maximal $\nu = \nu_U$ that did not create defects but resulted in stable asymptotic states in simulations of the short system. Plane waves and single MAWs (squares), multi-hump MAWs with two humps (triangles) and three humps (asterisks) have been observed at $\nu = \nu_U$. Data ν_U are taken from [25].

and into the defect chaos region. We stress this result because from the experimental observation of stable plane waves one cannot necessarily infer that the dynamics of the system may be reproduced by the CGLE with coefficients c_1, c_3 in the Benjamin–Feir stable region. The dashed curve denotes a subcritical instability. Only unstable upper branch MAWs exist to the left of this curve. For smaller ν the instability again turns supercritical and stable lower branch MAWs exist inside the dark shaded region. The thick solid curve gives the SN bifurcation for MAWs with $P = L$. The thin curves show the respective limits of MAWs with shorter period. Defects are expected beyond the SN [31,32] and the subcritical instability which well reproduces the data from numerical simulations [25] except at small ν . Simulations with $\nu \leq \nu_U$ resulted in modulations with a single hump (squares) or with two (triangles) or three (asterisks) humps of different size [25]. The latter two are observed above the SN of MAWs with $P = L$. Here the initial conditions select MAWs with shorter period which only coexist at small ν . The SN with $P = L$ nevertheless gives a lower bound for the formation of defects.

2.3. Instabilities of MAWs

A linear stability analysis of MAWs as in [32] yields the spectrum of eigenvalues as shown in Fig. 9 for a typical example. From Fig. 9 we conclude that for this example the entire spectrum in the infinite system will be confined to the left half-plane. Thus MAWs should

be found in experiments, that can be well described by the CGLE for appropriate control parameters. In this section we present a detailed study of the stability properties of MAWs. MAWs with a single hump per period P will be called “single MAWs”. Their existence domains were studied in the previous section. However, the effective interaction between adjacent periods of a single MAW can be repulsive or attractive (see Fig. 11). PD bifurcations (open squares) occur at the transitions from repulsive to attractive interaction [39]. There, new branches of MAWs with longer period but many humps per period emerge from the primary branch of single MAWs. We will call these solutions “multi-hump MAWs”. In their profile some humps gain more space and others are compressed in an alternating fashion. The new branches extend to larger c_3 than the corresponding single MAWs. Fig. 10 shows how these branches arrange in a system with four interacting humps ($L = 4P$). As long as the PD bifurcations are supercritical, the multi-hump MAWs are stable. They represent the saturated solution for attractive interaction between subsequent modulations. For large systems a whole sequence of PD bifurcations will lead to multi-hump MAWs with an overall period equal to the system size. Hence they appear as an erratic spatial sequence of humps and depressions. This spatial sequence propagates in a coherent fashion. We named these patterns multi-hump MAWs to emphasize the connection among the coherent structures.

Examples of these stable aperiodic patterns were already observed in numerical simulations. Montagne

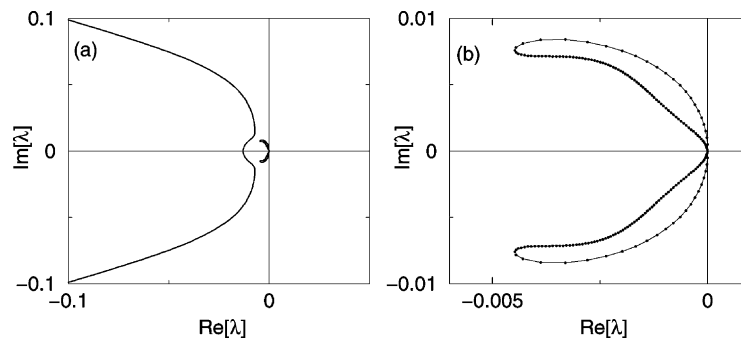


Fig. 9. (a) Spectrum of eigenvalues λ of a stable lower branch MAW. Parameters are $c_3 = 0.4$, $\nu = 0.184$, and $P = 2\pi/\nu$. (b) Blow-up of the leading part of the spectrum. The dots correspond to system size $L = 100P = 3415$ and have been calculated using the Bloch method [32,38].

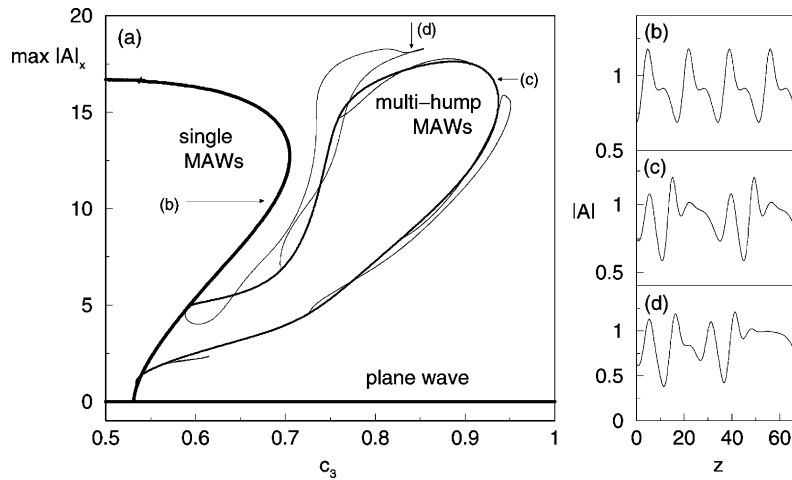


Fig. 10. (a) Bifurcation diagram for $\nu = 0.184$, $P = \pi/\nu$, and $L = 4P = 68.3$ hence four pulse-like modulations interact. The maximum of the amplitude gradient is plotted since the interaction causes pulse shifts and the amplitude of single humps changes little. Thicker lines correspond to smaller overall period of the modulation. Typical solutions are shown in (b)–(d) as indicated by arrows in (a).

et al. [24] denote this behavior as “frozen phase turbulence” while Torcini and coworkers [25] use the term “solutions of type β ”.

The observed coexistence of a large number of stable multi-hump MAWs results in a strong dependence of the final state on the initial conditions of the numerical simulation. Although each regular final configuration must be consistent with a particular single or multi-hump MAW it is difficult to predict how the selected final patterns depend on the initial conditions.

MAWs with large period P undergo a “splitting” instability as in the limit case $\nu = 0$ [32]. Roughly, the spatial profiles of these MAWs consist of a localized hump and a plane wave part. Since the extended plane wave is linearly unstable the splitting instability is reminiscent of the Eckhaus instability. It creates more humps on the plateau of the unstable MAW and reduces the period P of MAWs on average.

Fig. 11a and b represents cuts through the parameter space at fixed $\nu = 0.25$ and $c_3 = 0.5$, respectively.

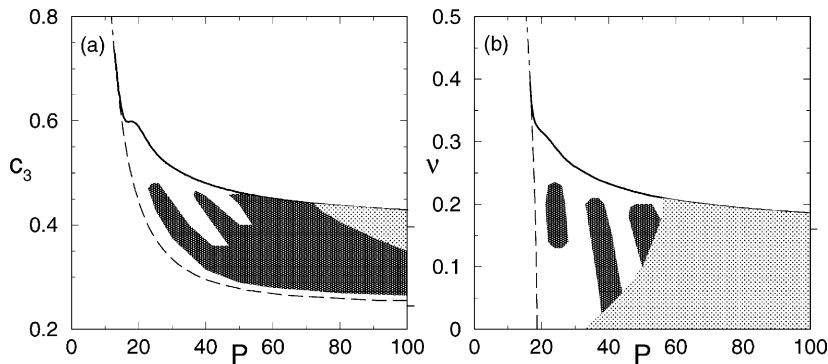


Fig. 11. Stability domain (dark area) of single MAWs for (a) $\nu = 0.25$, $L \rightarrow \infty$ and (b) $c_3 = 0.5$, $L \rightarrow \infty$. MAWs exist between supercritical HB (dashed curve) and SN (solid curve). The tick marks at the right frames give the asymptotic values for $P \rightarrow \infty$. The dot-dashed curve denotes the subcritical HB. MAWs are unstable to splitting within the light shaded domain at large P . Within the white domain at small P single MAWs are unstable to interaction.

They show the typical arrangement of stable and unstable parameter regions for single MAWs. Other examined cuts for $c_3 = 0.1, 0.2, 0.3, 0.4, 0.6,$ and 0.7 qualitatively show the same order.

The cut through parameter space c_3, ν, P at $\nu = 0.25$ is shown in Fig. 11a. The HB (dashed curve in the figure) approaches the Eckhaus instability for $P \rightarrow \infty$ as the lower bound of the existence domain. From above the domain is limited by the SN (solid curve). For small P (large c_3) the HB is subcritical and only unstable upper branch MAWs exist to the left. In the infinite system MAWs are found to be linearly stable for a broad range of parameters (dark shaded area). At low P the interaction instability occurs (white area), whereas at large P the long plateau of the MAW is unstable to splitting (light shaded area). For $c_3 < 0.45$ most random initial conditions will evolve to stable MAWs.

A cut perpendicular to the previous one is shown in Fig. 11b. Curves and shadings have the same meaning as discussed above. Starting from random initial conditions at $\nu > 0.1$ a transient may again lead to a stable MAW with local periods P inside the stable windows. At lower $\nu < 0.1$ the probability of approaching a stable configuration decreases since only a third of the previous stable P intervals remains. Below $\nu = 0.02$ no stable state can be prepared at all. Instead one observes wound-up phase chaos with an associated maximal Lyapunov exponent that increases for decreasing ν . As in the limit case $\nu = 0$ (phase chaos), the dynamics is driven by the attractive interaction and annihilation of localized modulations in competition with the splitting instability that produces new peaks in the modulations. In particular for decreasing ν , the splitting instability extends to shorter periods P and significantly overlaps with the interaction instability. With the above arguments many results obtained by numerical simulations of the CGLE can be well interpreted. In particular it has been observed in [25] for the same choice of parameters ($c_1 = 3.5$ and $c_3 = 0.5$) that the maximal Lyapunov exponent (averaged over many different initial conditions) is positive for $\nu = 0$ and decreases monotonously towards zero for increasing ν . Above $\nu = 0.09$ no chaotic solutions have been observed.

3. Defect formation in wound-up phase chaos

In this section the formation of defects and the resulting change of the average phase gradient are studied. For $\nu \neq 0$, the scenario of defect formation past the SN bifurcation of the relevant MAW is analogous to the previously studied case $\nu = 0$ [31,32], see Section 3.1. In particular, the dependence of the final selected average phase gradient ν_f on the initial value ν_i found in numerical simulations [24] can be interpreted. Section 3.2 is then devoted to the limit ν_M of wound-up phase chaos. For a certain range of parameters the limit ν_M is reproduced by means of the stability properties of MAWs at the SN bifurcation. These arguments work well for defect creation with $\nu > 0.1$. At smaller values of ν various instabilities (splitting and interaction) of MAWs compete and a general statement is more difficult, compare also [32].

3.1. Beyond the SN bifurcation

The role of the SN bifurcation for the dynamics has been studied in [31,32] for the limit case $\nu = 0$. For $\nu \neq 0$ we find similar behavior. Fig. 12 gives examples for $\nu = 0.25$ and $P = 2\pi/\nu$. Perturbations of a plane wave lead to defects only above the SN, whereas below the SN such perturbations have to be very large to overcome the saddle-type upper branch MAW.

There are no SNs for parameters below the SN corresponding to $P \rightarrow \infty$. Thus, starting from random initial conditions defects may only form at parameters above the SN of $P \rightarrow \infty$. The SN of $P \rightarrow \infty$ represents a lower bound for defect formation.

For large systems the formation of defects depends on the local period of initial perturbations in a similar way as for $\nu = 0$ [31,32]. The peak to peak distances of $\varphi_x(x, t)$ are used to determine local periods p . In that context, the following explanation of defect formation has been proposed. Defects are observed in the phase turbulent regime whenever local structures, similar to MAWs, with spatial periods p larger than P_{SN} occur in the system. Where P_{SN} denotes the period of the MAWs at the SN (that coincides with the maximal MAW-period) for the considered choice of parameters.

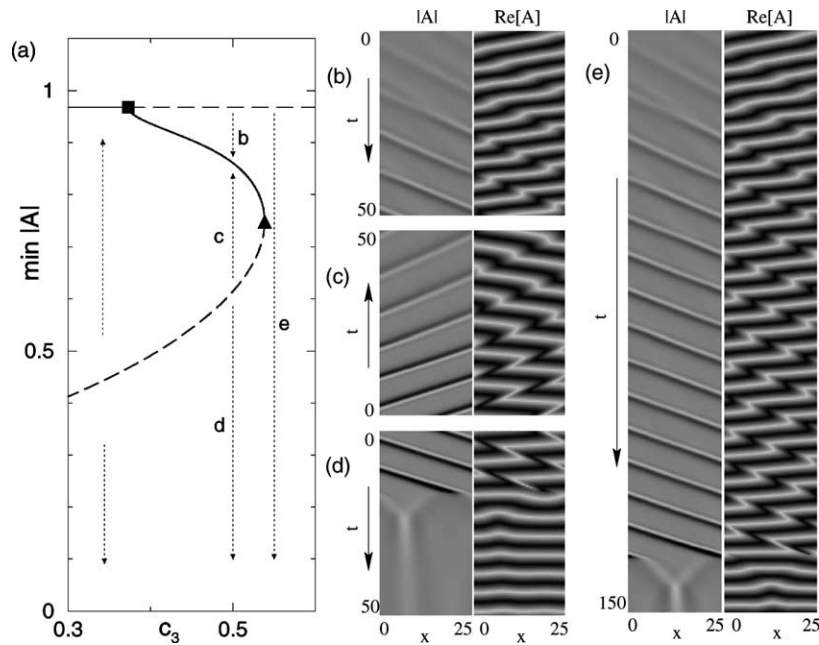


Fig. 12. (a) Bifurcation diagram as in Fig. 3 showing the minimum modulus of the MAWs. (b)–(e) Numerical simulations illustrate the dynamics near the SN corresponding to the arrows in (a). (b) Plane wave perturbed at one point and (c) unstable saddle-type MAW plus noise converge to the stable MAW. (d) Unstable saddle-type MAW plus a different realization of noise evolves to a defect that changes ν to 0. (e) As (b) but beyond the SN which makes defect formation possible for arbitrarily small perturbations of the plane wave. Note the long living transient of a noncoherent modulation. Parts (b)–(d) are at $c_3 = 0.5$ below the SN and (e) belongs to $c_3 = 0.55$ above the SN for $\nu = 0.25$ and $P = L = 2\pi/\nu = 25.13$.

For larger values of ν or c_3 the SN occurs for smaller P_{SN} as shown in Fig. 11. Therefore, at larger ν , c_3 local periods p beyond the SN and subsequent defect formation are more probable. In contrast to the case $\nu = 0$, there is only a short transient of phase chaos in the simulations with nonzero initial $\nu_i > \nu_M$. The distribution of local periods p of the perturbations is given by the realization of the noise in the initial condition. For local periods slightly above the relevant SN (as in Fig. 12e), the perturbation first increases to a modulation similar to MAWs and appears almost saturated for some transient time until finally a defect appears. This transient of defect formation becomes shorter as the distance to the SN grows. If initial conditions are prepared with $\nu_i \gg \nu_M$, then some local periods will be far beyond the corresponding SNs. The transients of defect formation are shorter in this case.

These two observations suggest an interpretation of the curve $\nu(t)$ representing the temporal evolution of

ν during transients with $\nu_i > \nu_M$ [24]. The larger the initial ν_i is chosen the smaller is the final value ν_f . The time scales of competing processes have to be considered. Local defect formation will not instantaneously effect distant spatial locations along the system. Instead the local change of the average phase gradient ν via a defect will take a transient time to relax over the entire system. For ν_i much larger than ν_M , defect formation happens on a short time scale and independently leads to defects at many different spatial locations before the relaxation of the decreased average phase gradient $\nu_f \ll \nu_M$ can stop defect formation. For ν_i just above ν_M defects form slowly and the reduced ν_f can relax the phase gradient at distant locations before other defects occur.

Let us now verify if the mechanisms proposed to explain defect formation in the phase chaos regime for solutions with $\nu \approx 0$ still hold for the wound-up phase chaos regime. For $\nu \approx 0$, defects form if and only if the period p of local structures is larger than

P_{SN} , where P_{SN} is the period for which a SN occurs at the chosen coefficients c_1 and c_3 [31,32]. We have considered two cuts in the parameter space at $c_3 = 0.5$ and $c_3 = 0.65$ and investigated the distributions of periods p for solutions with average phase gradient $\nu \sim \nu_M$. In particular, 50 realizations of a system of length $L = 512$ initialized as a plane wave with wavenumber ν plus noise in the amplitude and in the phase have been considered. Then these different initial conditions have been followed for an integration time $t = 500,000$ – $1,000,000$. The last part of the run has been examined in order to extract the length of the coherent structure with the maximal period p_{max} occurring during the evolution.

From these simulations we obtain the following: if defects occur then $p_{\text{max}} > P_{\text{SN}}$ in all observed cases. However, it is not true that a defect is formed any time we observe $p_{\text{max}} > P_{\text{SN}}$. If we let the system relax for a long time ($t = 500,000$) and measure p_{max} , then the number of initial conditions leading to a $p_{\text{max}} > P_{\text{SN}}$ without defect formation is noticeably reduced. For $c_3 = 0.65$ the maximal conserved phase gradient is $\nu_M \sim 0.1$. In the simulations we do not observe a defect for $\nu = 0.086$ and $\nu = 0.098$ but in the first case only 2% of all runs show $p_{\text{max}} > P_{\text{SN}}$, while in the latter case this percentage increases to 8%. Increasing ν the maximal period p_{max} increases and more and more situations with $p_{\text{max}} > P_{\text{SN}}$ are found upon approaching ν_M .

The difference to the $\nu = 0$ case may be explained by the coexistence of chaotic and stable not-chaotic attractors. Depending on the initial conditions, the solution of the CGLE can evolve towards one or the other. Therefore the system may exhibit local structures similar to multi-hump MAWs that possess SN bifurcations at parameter values larger than those of single MAWs (compare Fig. 10). In that case, some periods p may even exceed P_{SN} .

3.2. Limit of wound-up phase chaos

For random initial conditions with ν in the narrow range between the SN of $P \rightarrow \infty$ and the existence limit of MAWs (see Fig. 6), it depends on the specific realization of the noise whether a defect can form

or a stable MAW results. No defects form below the line $\nu_M(c_3)$. In order to understand this observed limit $\nu_M(c_3)$ of wound-up phase chaos, it is sufficient to consider the SNs of single MAWs.

Although initial conditions with large P beyond a SN could lead to defects, this is often prevented by the action of the splitting instability. Then the period is decreased before a defect can form. Following the SN curve in Fig. 11a and b one encounters a transition from SNs with a splitting instability at large P to SNs without this instability at short P . Defect formation in wound-up phase chaos with $\nu > 0.1$ occurs for parameters where the splitting instability is *not* present near the SN, i.e. above the dotted line in Fig. 13.

Fig. 13 summarizes the bounds found so far for the limit of wound-up phase chaos. The domain of stable plane waves at low c_3 is limited by the Eckhaus instability (thin curve). Within the shaded area only supercritical HBs of different period P occur but no SNs. This area is limited by the lowest SN curve of $P \rightarrow \infty$ (thick solid curve). No defects do form from random initial conditions within the shaded area. The dashed curve denotes the upper limit of the existence domain of MAWs with any period. SN bifurcations exist in the window between this dashed curve and the thick solid curve for the SN with $P \rightarrow \infty$. Defects will always form for any choice of initial conditions at parameters above the dashed curve. The dotted curve gives the transition from active (below) to inactive (above) splitting modes at the SN. This transition is computed by linear stability analysis along cuts like in Fig. 11. Splitting inhibits defect formation below this dotted curve. Filled circles correspond to ν_M obtained from numerical simulations as in [25]. Diamonds refer to the transition from chaotic (below) to nonchaotic (above) asymptotic states.

The SN for $P \rightarrow \infty$ (thick solid curve) is a lower bound for defect formation which also holds in the limit $\nu = 0$. The point L_1 marks the transition from phase to defect chaos studied earlier [31,32].

As long as the dynamics is regular ($\nu > 0.1$), the upper bound for the limit (onset of splitting at SN, dotted curve) of wound-up phase chaos reproduces well the numerical observations. For chaotic states with $\nu < 0.1$ defect formation eventually becomes possi-

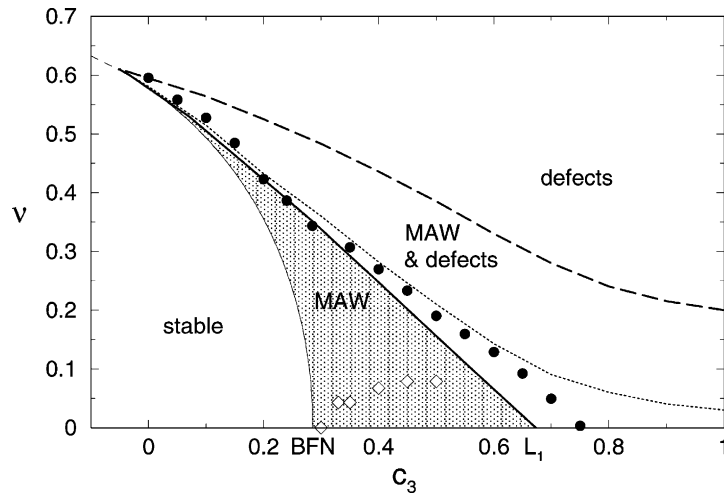


Fig. 13. Theoretical bounds for $v_M(c_3)$ (filled circles): SN of $P \rightarrow \infty$ as lower bound (thick solid curve) and the presence of splitting at SN as upper bound (dotted curve). The thick dashed curve limits the existence of MAWs (compare Fig. 6), other curves as in Fig. 2. See text for details.

ble even despite the presence of the splitting instability. This coincides with the increasing weight of the instability of single MAWs to attractive interaction of subsequent amplitude peaks.

4. Experimental observations

A variety of experimental observations in quasi one-dimensional geometries can be well interpreted by MAWs. These systems shall also serve for testing further properties of MAWs [40].

- (i) For the oscillatory instability of Rayleigh–Bénard convection patterns in an annular cell, Janiaud et al. report long living transients of modulated waves that eventually cause defects [4]. The underlying Eckhaus instability was found to be subcritical. Then, we expect the modulation to grow roughly exponentially, whereas the long transient of an almost saturated modulation is similar to the dynamics near the SN bifurcation as shown in Fig. 12e. In the latter case the Eckhaus instability is supercritical and stable MAWs may exist for nearby values of the experimental parameters, see also the discussion in [41]. In all cases a single pulse-shaped modulation with the period equal to

the cell length was present in the system and led to a defect. The excitation of several modulations per cell and thereby smaller period can stabilize the modulated pattern and provide more examples of the dynamics near the SN bifurcation.

- (ii) Hydrothermal waves have been studied in ring-shaped cells [6] as well as in linear cells [5,7,8]. Mukolobwicz et al. report a supercritical Eckhaus instability, stable MAWs with the period equal to the cell length and defect formation after a parameter change [6]. Garnier et al. observe modulated waves with both the wavenumber and the period of modulations being selected by one of the longitudinal boundaries [7]. Thermal or mechanical forcing at the boundary may yield more insight into the multistability of the two-parameter family of MAWs.
- (iii) In rotating Rayleigh–Bénard convection Liu et al. observe the subcritical Eckhaus instability of a traveling wave sidewall mode [10]. The authors suggest higher order corrections to the CGLE in order to explain the observed discrepancy between the linear group velocity and the observed velocity of finite wavelength perturbations. However, this difference already follows from the linear analysis of the Eckhaus

instability (see Footnote 1) and can be used as a test for the assumed coefficients of the CGLE.

- (iv) For the Taylor–Dean system Mutabazi and co-workers report a stable MAW that they called “triplet state” because of the length scale ratio of modulation and underlying wave [11]. They also observe the formation of defects. Clearly the triplet state is just one realization of the two-parameter family of MAWs.
- (v) Finally we mention the heated wire convection [9], internal waves [12] and the oscillatory variant of the Belousov–Zhabotinsky reaction [13] where further investigations of the observed Eckhaus instabilities may also reveal MAWs.

5. Discussion

The bifurcation analysis of MAWs has been extended to nonzero average phase gradient ($\nu \neq 0$). Small amplitude MAWs (“lower branch”-MAWs) of specific spatial period P exist between a supercritical HB and a SN bifurcation. The HB asymptotically reaches the Eckhaus instability from above as P goes to infinity. MAWs are a direct consequence of the Eckhaus instability of plane waves; they are obtained by a computer-assisted nonlinear analysis of this instability. We encounter SNs with decreasing values of P as c_1 , c_3 and ν are increased. These SNs govern the formation of defects from random initial conditions as well as many aspects of the evolution of wound-up phase chaos. The SNs bound the existence region of MAWs in the Eckhaus unstable regime.

A linear stability analysis of MAWs revealed that they can be linearly stable even in systems of infinite size. These domains are limited by the interaction instability at low and the splitting instability at high values of the spatial period P of the MAW. The competition of the two instabilities drives wound-up phase chaos and determines the degree of chaoticity of the dynamics. For fixed coefficients c_1 and c_3 , the SN associated to $P \rightarrow \infty$ occurs at the lowest value of ν . This SN establishes a “lower” bound for defect formation and thereby for the limit ν_M of wound-up phase chaos. The splitting instability can inhibit de-

fect formation if the SN occurs at large P hence defects are created more frequently for parameters above a second curve where the splitting instability vanishes at the SN. Thereby an “upper” bound for the limit ν_M of wound-up phase chaos is obtained. Earlier numerical observations on $\nu_M(c_3)$ are well reproduced for $\nu > 0.1$, respectively, small c_3 . For $\nu < 0.1$, the description of phase chaos relies on considerations similar to those already discussed in the limit case $\nu = 0$ [31,32]. Finally, several experimental observations were interpreted in terms of MAWs.

Acknowledgements

We acknowledge fruitful discussions with M. van Hecke, N. Garnier, F. Daviaud, W. van de Water and L. Kramer. AT was partially supported by the MURST-COFIN00 Grant “Chaos and localization in classical and quantum mechanics”.

References

- [1] Y. Kuramoto, *Chemical Oscillations, Waves and Turbulence*, Springer, Berlin, 1984; P. Manneville, *Dissipative Structures and Weak Turbulence*, Academic Press, San Diego, 1990; T. Bohr, M.H. Jensen, G. Paladin, A. Vulpiani, *Dynamical Systems Approach to Turbulence*, Cambridge University Press, Cambridge, 1998.
- [2] M.C. Cross, P.C. Hohenberg, *Rev. Mod. Phys.* 65 (1993) 851.
- [3] W. Eckhaus, *Studies in Nonlinear Stability Theory*, Springer, New York, 1965.
- [4] B. Janiaud, A. Pumir, D. Bensimon, V. Croquette, H. Richter, L. Kramer, *Physica D* 55 (1992) 269.
- [5] F. Daviaud, J.M. Vince, *Phys. Rev. E* 48 (1993) 4432.
- [6] N. Mukolobwiz, A. Chiffaudel, F. Daviaud, *Phys. Rev. Lett.* 80 (1998) 4661.
- [7] N. Garnier, A. Chiffaudel, F. Daviaud, A. Prigent, Nonlinear dynamics of waves and modulated waves in 1D thermocapillary flows. I. General presentation and periodic solutions, *Physica D* (2003) 174 (2003) 1–29.
- [8] N. Garnier, A. Chiffaudel, *Phys. Rev. Lett.* 86 (2001) 75.
- [9] J.M. Vince, M. Dubois, *Physica D* 102 (1997) 93.
- [10] Y. Liu, R.E. Ecke, *Phys. Rev. Lett.* 78 (1997) 4391; Y. Liu, R.E. Ecke, *Phys. Rev. E* 59 (1999) 4091.
- [11] I. Mutabazi, J.J. Hegesth, C.D. Andereck, J.E. Wesfreid, *Phys. Rev. Lett.* 64 (1990) 1729; P. Bot, O. Cadot, I. Mutabazi, *Phys. Rev. E* 58 (1998) 3089; P. Bot, I. Mutabazi, *Eur. Phys. J. B* 13 (2000) 141.
- [12] A. Wierschem, H. Linde, M.G. Velarde, *Phys. Rev. E* 62 (2000) 6522.

- [13] Q. Ouyang, J.M. Flesselles, *Nature* 379 (1996) 143;
Q. Ouyang, H.L. Swinney, G. Li, *Phys. Rev. Lett.* 84 (2000) 1047;
L.Q. Zhou, Q. Ouyang, *Phys. Rev. Lett.* 85 (2000) 1650.
- [14] I.S. Aranson, L. Kramer, The world of the complex Ginzburg–Landau equation, *Rev. Mod. Phys.* 74 (2002) 99.
- [15] J.T. Stuart, R.C. DiPrima, *Proc. R. Soc. London, Ser. A* 362 (1978) 27.
- [16] I.S. Aranson, L. Aranson, L. Kramer, A. Weber, *Phys. Rev. A* 46 (1992) R2992.
- [17] A. Weber, L. Kramer, I.S. Aranson, L. Aranson, *Physica D* 61 (1992) 279.
- [18] M. Büttiker, H. Thomas, *Phys. Rev. A* 24 (1981) 2635.
- [19] R. Conte, M. Musette, *Physica D* 69 (1993) 1.
- [20] A.V. Porubov, M.G. Velarde, *J. Math. Phys.* 40 (1999) 884.
- [21] H.-C. Chang, E.A. Demekhin, D.I. Kopelevich, *Physica D* 63 (1993) 299.
- [22] D.E. Bar, A.A. Nepomnyashchy, *Physica D* 86 (1995) 586.
- [23] A. Pumir, B.I. Shraiman, W. van Saarloos, P.C. Hohenberg, H. Chaté, M. Hohen, in: C.D. Andereck, F. Hayot (Eds.), *Ordered and Turbulent Patterns in Taylor–Couette Flow*, Plenum Press, New York, 1992, p. 173.
- [24] R. Montagne, E. Hernández-García, M. San Miguel, *Phys. Rev. Lett.* 77 (1996) 267;
R. Montagne, E. Hernández-García, A. Amengual, M. San Miguel, *Phys. Rev. E* 55 (1997) 151.
- [25] A. Torcini, *Phys. Rev. Lett.* 77 (1996) 1047;
A. Torcini, H. Frauenkron, P. Grassberger, *Phys. Rev. E* 55 (1997) 5073.
- [26] G. Hager, Quasiperiodische Lösungen der eindimensionalen komplexen Ginzburg–Landau Gleichung, Diploma Thesis, University of Bayreuth, Germany, 1996.
- [27] B.I. Shraiman, A. Pumir, W. van Saarloos, P.C. Hohenberg, H. Chaté, M. Hohen, *Physica D* 57 (1992) 241.
- [28] H. Chaté, *Nonlinearity* 7 (1994) 185;
H. Chaté, in: P.E. Cladis, P. Palfy-Muhoray (Eds.), *Spatio-Temporal Patterns in Nonequilibrium Complex Systems*, Addison-Wesley, Reading, MA, 1995, p. 33.
- [29] H. Sakaguchi, *Prog. Theor. Phys.* 84 (1990) 792.
- [30] D.A. Egolf, H.S. Greenside, *Phys. Rev. Lett.* 74 (1995) 1751.
- [31] L. Bruschi, M.G. Zimmermann, M. van Hecke, M. Bär, A. Torcini, *Phys. Rev. Lett.* 85 (2000) 86.
- [32] L. Bruschi, A. Torcini, M. van Hecke, M.G. Zimmermann, M. Bär, *Physica D* 160 (2001) 127.
- [33] W. van Saarloos, P.C. Hohenberg, *Physica D* 56 (1992) 303; erratum 69 (1993) 209.
- [34] M. van Hecke, *Phys. Rev. Lett.* 80 (1998) 1896.
- [35] M. van Hecke, M. Howard, *Phys. Rev. Lett.* 86 (2001) 2018.
- [36] E. Doedel, A. Champneys, T. Fairgrieve, Y. Kusnetsov, B. Sandstede, X. Wang, AUTO97: continuation and bifurcation software for ordinary differential equations, Concordia University, Montreal, 1997.
- [37] M. Kness, L. Tuckerman, D. Barkley, *Phys. Rev. A* 46 (1992) 5054.
- [38] N.W. Ashcroft, N.D. Mermin, *Solid State Physics*, Holt, Rinehart & Winston, New York, 1976;
P. Collet, J.-P. Eckmann, *Instabilities and Fronts in Extended Systems*, Princeton University Press, Princeton, NJ, 1990.
- [39] M. Or-Guil, I.G. Kevrekidis, M. Bär, *Physica D* 135 (2000) 154.
- [40] M. van Hecke, Coherent and incoherent structures in systems described by the 1D CGLE: experiments and identification. *Physica D* 174 (2003) 134–151.
- [41] B. Janiud, E. Guyon, D. Bensimon, V. Croquette, in: F. Busse, L. Kramer (Eds.), *Nonlinear Evolution of Spatio-Temporal Structures in Dissipative Continuous Systems*, NATO ASI Series B, vol. 225, Plenum Press, New York, 1990.